Journal of Alloys and Compounds 508 (2010) 507–511

Contents lists available at ScienceDirect

Journal of Alloys and Compounds

journal homepage: www.elsevier.com/locate/jallcom

Synthesis of $(1-x)ZnAl_2O_4$–$xTiO_2$ microwave dielectric ceramics by molten-salt process

Wen Lei, Wen-Zhong Lu*, Xiao-Chuan Wang, Shuai Wan

Department of Electronic Science and Technology, Huazhong University of Science and Technology, 1037 Luoyu Road, Wuhan, Hubei 430074, China

ARTICLE INFO

Article history:
Received 31 August 2009
Received in revised form 14 August 2010
Accepted 26 August 2010

Keywords:
$ZnAl_2O_4$-based ceramics
Molten-salt process
Dielectric properties
Sintering characteristics

ABSTRACT

Sintering characteristic, phase compositions, microstructures and microwave dielectric properties of $(1-x)ZnAl_2O_4$–$xTiO_2$ ceramics synthesized by LiCl and $ZnCl_2$ molten-salt were investigated. Molten-salt process can prepare smaller and more homogenous grains than the solid-state reaction method, and can lower effectively its densification temperature. Besides $ZnAl_2O_4$ spinel and rutile main phase, sometimes $Zn_2Ti_3O_8$ phase could exist in the ceramic system, which is closely related to TiO_2 content or sintering temperature. When x value is equal to 0.25, a stable-temperature $(1-x)ZnAl_2O_4$–$xTiO_2$ ceramics calcined at 900 °C in LiCl molten-salt and sintered at 1300 °C in air can be obtained, and exhibits microwave dielectric properties with an ε_r value of 9.8, a $Q{\cdot}f$ value of 27,000 GHz, and a τ_f value of −7.1 ppm/°C. $ZnCl_2$ molten-salt can improve significantly the quality factor ($Q{\cdot}f$ = 56,440 GHz), however, deteriorate the temperature coefficient of resonant frequency (τ_f = −25.4 ppm/°C) of the ceramics.

1. Introduction

For application to millimeter-wave systems, microwave dielectric materials require a low dielectric constant (ε_r) to minimize the cross-coupling effect with conductors and shorten the time for the electronic signal transition, a high quality factor ($Q{\cdot}f$) to increase their selectivity, and a near-zero temperature coefficient of resonant frequency (τ_f) to ensure the stability of the frequency against temperature changes [1].

In 2005, Surendran et al. [2] suggested that $ZnAl_2O_4$–TiO_2 spinel-based ceramics have outstanding electrical insulating properties, thermochemical stability properties, thermal-expansion properties, and they can be proposed as potential microwave substrate and antenna materials substituting for the commonly used alumina substrate. Lei et al. [3–5] had studied the sintering processes and microwave dielectric properties of $(1-x)ZnAl_2O_4$–$xTiO_2$ ceramics, and found that the optimal properties can be achieved in $(1-x)ZnAl_2O_4$–$xTiO_2$ (x = 0.21) ceramics calcined at 1150 °C and sintered at 1500 °C for 3 h at a heating rate of 5 °C/min, with ε_r value of 11.6, $Q{\cdot}f$ value of 74,000 GHz (at about 6.5 GHz), and τ_f value of −0.4 ppm/°C.

However, the sintering temperature of the $(1-x)ZnAl_2O_4$–$xTiO_2$ (x = 0.21) ceramics is too high and needs to be decreased. $ZnAl_2O_4$ fine powders can be easily synthesized through wet chemical routes such as the coprecipitated products, citric acid route, Pechini method, hydrothermal synthesis method, sol–gel method and evaporation-induced self-assembly method [6,7], and sintering temperature can be reduced significantly. Furthermore, molten-salt process is also a well established low temperature synthesis technique that has recently attracted increasing interest. It has been used to synthesize low melting electroceramic powders and high temperature complex oxide powders [8], however, are not still found for $ZnAl_2O_4$-based ceramics preparation. In this study, the effects of molten-salt process on sintering characteristics, phase compositions, microstructures and microwave dielectric properties of $(1-x)ZnAl_2O_4$–$xTiO_2$ ceramics were investigated.

2. Experimental procedure

Reagent-grade ZnO, Al_2O_3, TiO_2 (Rutile), LiCl and $ZnCl_2$ powders were used as raw materials. The weight ratio of LiCl (or $ZnCl_2$) salt to $(1-x)ZnAl_2O_4$–$xTiO_2$ (x = 0.21, 0.23 and 0.25) powder is 3:1. The $(1-x)ZnAl_2O_4$–$xTiO_2$ powder added salts were milled with agate balls in ethanol for 3 h at a speed of 360 rpm (rotations per minute). The slurry was dried at 80 °C in an infrared stove, and then calcined in air at 900 °C for 3 h. The molten-salts were removed from the products by washing several times with hot deionized water until the filtrate gave no reaction with silver nitrate solution. Then, after drying again, to the calcined powders, 7 wt.% polyvinyl alcohol was added, whose concentration in the aqueous solution was 5 wt.%, and a binder was uniaxially pressed into the samples with dimensions of 20 mm in diameter and about 10 mm in height under a pressure of 150 MPa. After sintered at 1250–1425 °C for 3 h at a heating rate of 5 °C/min in air, these samples were cooled at a rate of 2 °C/min up to 1000 °C and then they were furnace cooled.

The particle size was tested using laser particle size analyzer (Winner 2000). The crystalline phases were analyzed by means of the X-ray diffraction method using Cu Kα radiation (XRD, X'Pert PRO, PANalytical B.V., the Netherlands). The microstructure observation was performed by field scanning electron microscope (FSEM, Sirion 200, FEI, the Netherlands). The bulk density of the sintered pellets was measured

* Corresponding author. Tel.: +86 27 87542594; fax: +86 27 87543134.
E-mail address: lwz@mail.hust.edu.cn (W.-Z. Lu).

0925-8388/$ – see front matter
doi:10.1016/j.jallcom.2010.08.104

using the Archimedes method. The permittivity (ε_r) and the unloaded $Q\cdot f$ value were measured in the TE011 mode by Hakki and Coleman method [9] using an Advantest R3767C network analyzer and parallel silver boards. The temperature coefficient of resonant frequency (τ_f) in the temperature range of 20–80 °C was calculated by formula (1):

$$\tau_f = \frac{f_2 - f_1}{f_1(T_2 - T_1)} \quad (1)$$

where f_1 and f_2 represent the resonant frequencies at T_1 and T_2, respectively.

3. Results and discussions

3.1. Powder particle size

Fig. 1 illustrates particle size distributions of the raw powders and composite powders synthesized at 900 °C for 3 h in LiCl or $ZnCl_2$ salt. Only one peak at about 2 μm appears for ZnO and TiO_2 raw powders, while four peaks for Al_2O_3 starting powder can be observed, as shown in Fig. 1(a). After ZnO reacting with Al_2O_3 and TiO_2 powders in molten-salt, particle size distributions of composite powders are similar to that of the Al_2O_3 starting powder (see Fig. 1(b)), which indicates that Al_2O_3 is used as a "template" due to its solubility in the two kinds of molten-salt both greatly lower than that of ZnO and TiO_2 [8].

Table 1 shows average particle diameter of the raw powders and composite powders synthesized at 900 °C for 3 h in LiCl or $ZnCl_2$ salt. D_{av} value of the $(1-x)ZnAl_2O_4–xTiO_2$ ($x = 0.21$) powder (18.83 μm) prepared in LiCl is lower than that of Al_2O_3 raw powder (27.75 μm) because Al_2O_3 particles partly solute in the molten-salt. As the x value increases to 0.25, $(1-x)ZnAl_2O_4–xTiO_2$ particle size grows which indicates that TiO_2 can improve ion diffusivity and promote the particle growth. Compared with $(1-x)ZnAl_2O_4–xTiO_2$ ($x = 0.25$) powder in LiCl molten-salt, the powder in $ZnCl_2$ molten-salt has smaller D_{av} value (15.36 μm), possibly because Al_2O_3 powder has higher solubility in the latter.

Table 1
Average particle diameter (D_{av}) of the raw powders and composite powders synthesized at 900 °C for 3 h in LiCl or $ZnCl_2$ salt.

Powder	Molten-salt	D_{av} (μm)
ZnO	–	2.40
Al_2O_3	–	27.75
TiO_2	–	1.94
$0.79ZnAl_2O_4–0.21TiO_2$	LiCl	18.83
$0.75ZnAl_2O_4–0.25TiO_2$	LiCl	27.75
$0.75ZnAl_2O_4–0.25TiO_2$	$ZnCl_2$	15.36

3.2. XRD analysis

XRD patterns of $(1-x)ZnAl_2O_4–xTiO_2$ powders synthesized at 900 °C for 3 h in LiCl salt are shown in Fig. 2. $ZnAl_2O_4$ spinel and $Li_{2x}Zn_{(1-x)}Ti_3O_8$ phases are included in the $(1-x)ZnAl_2O_4–xTiO_2$ ($x = 0.21$) powder (see Fig. 2(a)). When x value reaches over 0.23, a new rutile phase appears in the $(1-x)ZnAl_2O_4–xTiO_2$ system (see Fig. 2(b) and (c)). Moreover, X-ray intensity of the $Li_{2x}Zn_{(2-x)}Ti_3O_8$ and rutile phase enhances gradually with the increase of TiO_2 content, as shown in Fig. 2. Formation of $Li_{2x}Zn_{(2-x)}Ti_3O_8$ phase can be expressed as follows:

$$2xLi^+ + (2-x)Zn^{2+} + 3Ti^{4+} + 8O^{2-} \rightarrow Li_{2x}Zn_{(2-x)}Ti_3O_8 \quad (2)$$

It is known from formula (2) that an increase in Ti^{4+} ions are helpful to form $Li_{2x}Zn_{(2-x)}Ti_3O_8$ phase, at the same time, Li^+ and Zn^{2+} ions are also required. In LiCl molten-salt, Li^+ ions are enough, however, Zn^{2+} ions added are limited. Therefore, as the amount of TiO_2 increases, $Li_{2x}Zn_{(2-x)}Ti_3O_8$ phase increases gradually. When Zn^{2+} ions run out, Li^+ ions could not form a kind of stable reac-

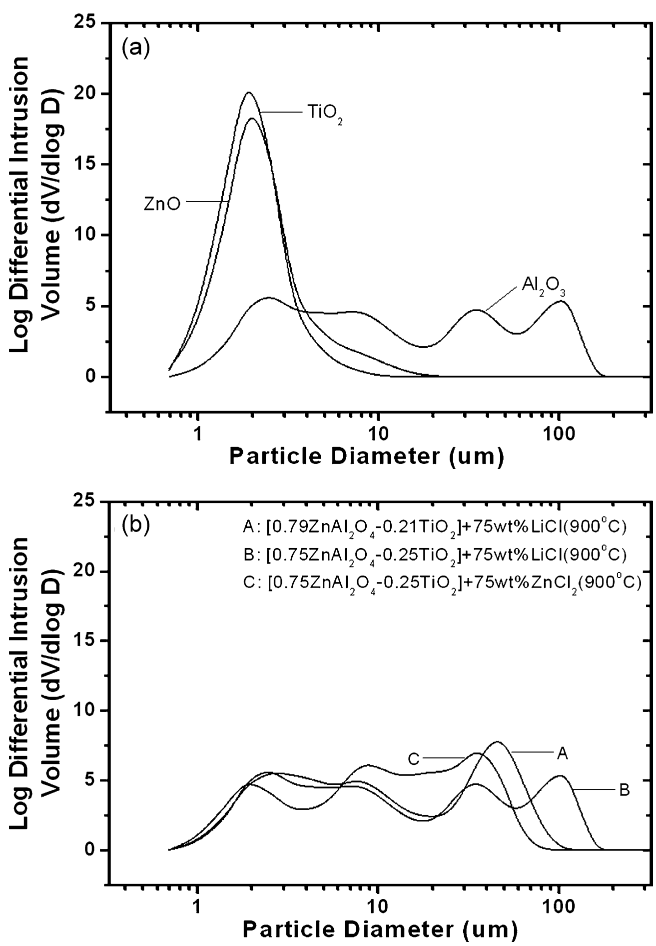

Fig. 1. Particle size distributions of (a) the raw powders and (b) composite powders synthesized at 900 °C for 3 h in LiCl or $ZnCl_2$ salts.

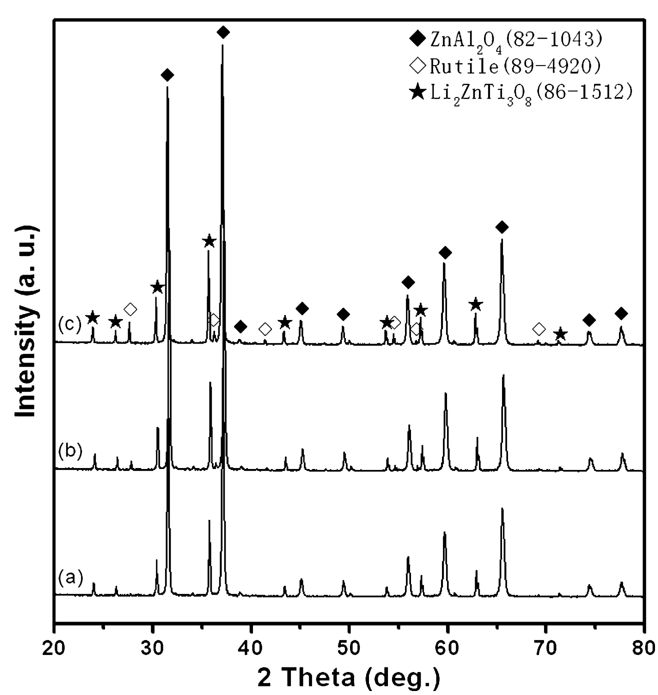

Fig. 2. XRD patterns of $(1-x)ZnAl_2O_4–xTiO_2$ powders synthesized at 900 °C for 3 h in LiCl salt: (a) $x = 0.21$; (b) $x = 0.23$; (c) $x = 0.25$.

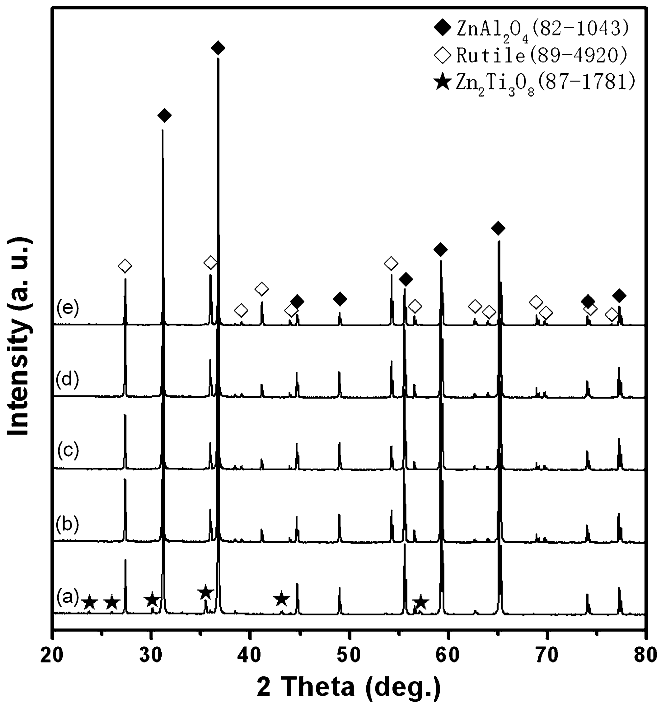

Fig. 3. XRD patterns of $(1-x)ZnAl_2O_4$–$xTiO_2$ ceramics calcined at 900 °C for 3 h in LiCl salt and sintered at different temperatures for 3 h: (a) $x = 0.21$, 1425 °C; (b) $x = 0.23$, 1300 °C; (c) $x = 0.25$, 1250 °C; (d) $x = 0.25$, 1300 °C; (e) $x = 0.25$, 1400 °C.

tant with Ti^{4+} ions during the cooling process, and redundant Ti^{4+} ions exist finally as rutile phase. The X-ray intensity of any phase is proportional to the relative volume fraction of the phase [3], therefore, an increase in TiO_2 content results in enhancement in X-ray intensity of the $Li_{2x}Zn_{(2-x)}Ti_3O_8$ and rutile phase, as shown in Fig. 2.

Fig. 3 shows XRD patterns of $(1-x)ZnAl_2O_4$–$xTiO_2$ ceramics calcined at 900 °C for 3 h in LiCl salt and sintered at different temperatures for 3 h. It seems that phase composition in the $(1-x)ZnAl_2O_4$–$xTiO_2$ system is only relative to TiO_2 content and independent of sintering temperature, as shown in Fig. 3. When x value is equal to 0.21, $ZnAl_2O_4$ spinel, rutile and $Zn_2Ti_3O_8$ phases (Li^+ ions in $Li_{2x}Zn_{(2-x)}Ti_3O_8$ phase vaporize easily over 1000 °C [10]) can be observed in the ceramics, while $Zn_2Ti_3O_8$ phase disappears for $x \geq 0.23$, because TiO_2 can improve ion diffusion and promote Zn^{2+} ion reaction with Al^{3+} ion to form $ZnAl_2O_4$. As the sintering temperature increases, the X-ray intensity of rutile phase in the $(1-x)ZnAl_2O_4$–$xTiO_2$ ($x = 0.25$) ceramics enhances gradually and that of $ZnAl_2O_4$ spinel phase weakens progressively, as shown in Fig. 3(c)–(e), because the TiO_2 grains grow easily with the increasing of the sintering temperature [3].

Fig. 4 represents the XRD patterns of $(1-x)ZnAl_2O_4$–$xTiO_2$ ($x = 0.25$) powder synthesized at 900 °C for 3 h in $ZnCl_2$ salt and ceramics sintered at different temperatures for 3 h. It can be observed that $ZnAl_2O_4$ spinel, rutile and $Zn_2Ti_3O_8$ phases exist in the $(1-x)ZnAl_2O_4$–$xTiO_2$ ($x = 0.25$) powder, as shown in Fig. 4(a). When the sintering temperature is 1300 °C, the phase composition in the ceramics is the same as that in the powder, and $Zn_2Ti_3O_8$ phase disappears until 1450 °C, as shown in Fig. 4(b).

3.3. Microstructures

Fig. 5 shows scanning electron micrographs of $(1-x)ZnAl_2O_4$–$xTiO_2$ ceramics prepared by the solid-state reaction and molten-salt process. Compared with the microstructure of $(1-x)ZnAl_2O_4$–$xTiO_2$ ($x = 0.21$) ceramics synthesized by

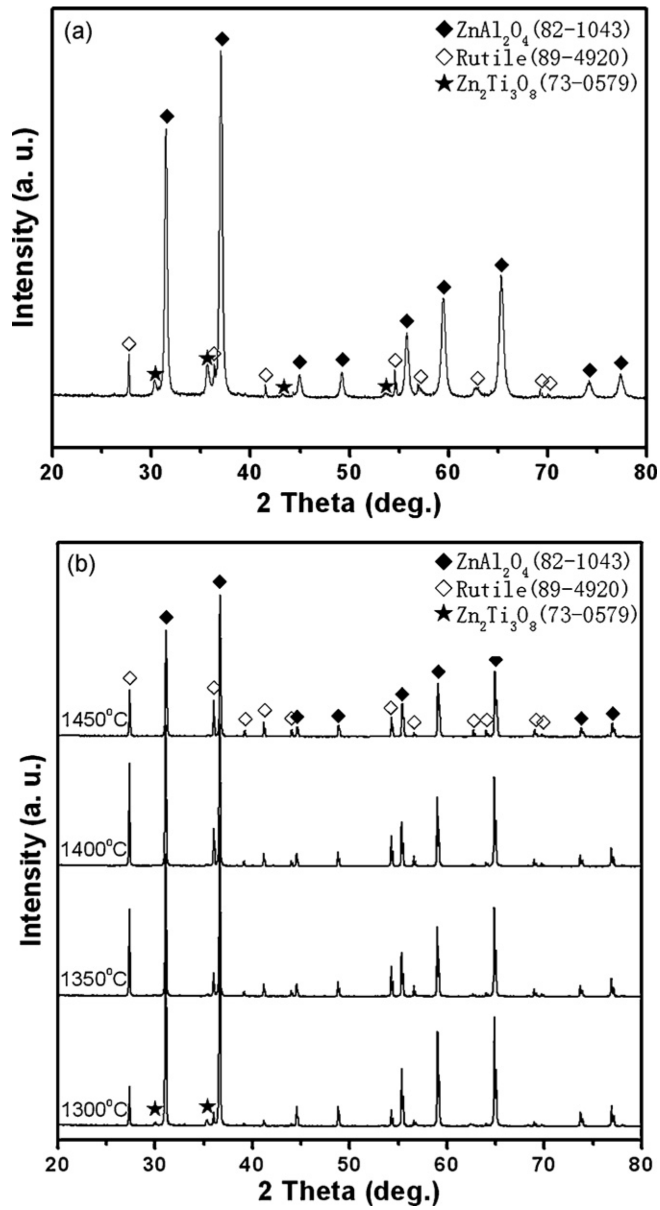

Fig. 4. XRD patterns of $(1-x)ZnAl_2O_4$–$xTiO_2$ ($x = 0.25$) (a) powder synthesized at 900 °C for 3 h in $ZnCl_2$ salt and (b) ceramics sintered at different temperatures for 3 h.

the solid-state reaction with the bigger rutile grains (>50 μm) and the smaller $ZnAl_2O_4$ grains (about 5 μm) [5] (see Fig. 5(a)), that of the ceramics prepared by LiCl molten-salt exhibits some smaller and more homogenous grains (see Fig. 5(b)). When x value reaches 0.25, the rutile grains grow quickly (see Fig. 5(c)). Moreover, the average size of larger rutile grains in the $(1-x)ZnAl_2O_4$–$xTiO_2$ ($x = 0.25$) ceramics synthesized by $ZnCl_2$ molten-salt increases further (see Fig. 5(d)), compared with that in Fig. 5(c).

3.4. Microwave dielectric properties

Density and microwave dielectric properties of $(1-x)ZnAl_2O_4$–$xTiO_2$ ceramics are shown in Table 2. LiCl and $ZnCl_2$ molten-salt process can lower the densification temperature of $(1-x)ZnAl_2O_4$–$xTiO_2$ ceramics. In comparison to $(1-x)ZnAl_2O_4$–$xTiO_2$ ($x = 0.21$) ceramics prepared by the solid-state reaction (No. 1), the ceramics synthesized by LiCl molten-salt process (No. 2) has lower bulk density, ε_r and $Q{\cdot}f$ value, and more negative τ_f value. On one hand, Li^+ ions vaporize easily

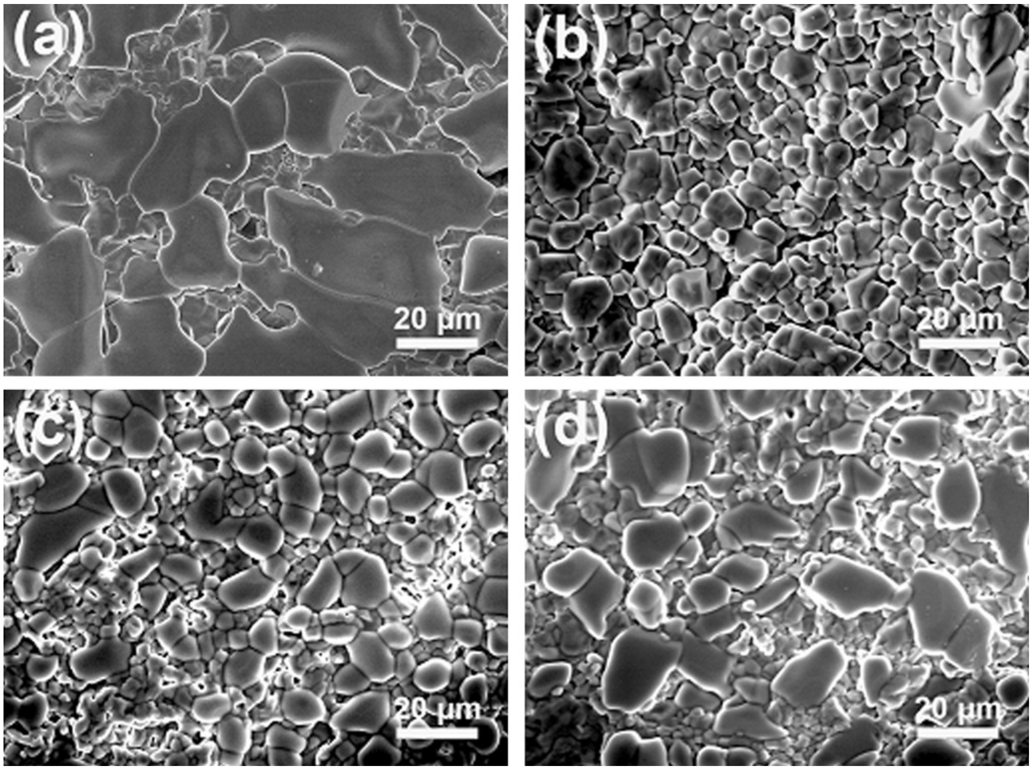

Fig. 5. Scanning electron micrographs of $(1-x)ZnAl_2O_4$–$xTiO_2$ ceramics: (a) $x = 0.21$, solid-state reaction, 1500 °C; (b) $x = 0.21$, LiCl salt, 1425 °C; (c) $x = 0.25$, LiCl salt, 1300 °C; (d) $x = 0.25$, $ZnCl_2$ salt, 1350 °C.

Table 2
Density and microwave dielectric properties of $(1-x)ZnAl_2O_4$–$xTiO_2$ ceramics.

No.	x	Molten-salt	T_{cal} (°C)	T_{sint} [a] (°C)	ε_r	$Q{\cdot}f$ (GHz)	τ_f (ppm/°C)	ρ (g/cm^3)
1	0.21	–	1150	1500	11.6	74,000	−0.4	4.42
2	0.21	LiCl	900	1425	10.0	39,970	−19.7	4.13
3	0.25	LiCl	900	1300	9.8	27,000	−7.1	4.15
4	0.25	$ZnCl_2$	900	1350	10.0	56,440	−25.4	4.39

[a] T_{sint} is densification temperature.

over 1000 °C to form micropores, on the other hand, as the grain size reduces, the number of triangular grain boundary increases, therefore micropores increase and bulk density decreases. At the same time, an increase in micropores leads to reduction in ε_r and $Q{\cdot}f$ values. Moreover, the amount of TiO_2 phase with highly positive τ_f value in the $(1-x)ZnAl_2O_4$–$xTiO_2$ ($x = 0.21$) system synthesized by LiCl molten-salt process reduces due to formation of $Zn_2Ti_3O_8$ second phase, which results in more negative τ_f value on the basis of the mixing rule [3]. When x value increases from 0.21 to 0.25, $Zn_2Ti_3O_8$ second phase disappears (see Fig. 3(a)) and the amount of TiO_2 phase in the system increases, therefore, the τ_f value can be adjusted to near zero (−7.1 ppm/°C) and densification temperature can be lowered from 1425 to 1300 °C. Although TiO_2 content in No. 3 is more than that in No. 1, the τ_f value of the former is slightly lower than that of the latter, which indicates that Ti^{4+} ions in the system prepared by LiCl molten-salt process could diffuse more easily into the crystal lattice of the $ZnAl_2O_4$ spinel phase. $Zn_2Ti_3O_8$ has the same spinel structure as $ZnAl_2O_4$, however, their lattice constants have great difference, so they can only form limited solid solution. When LiCl was replaced by $ZnCl_2$ molten-salt, the τ_f value of the $(1-x)ZnAl_2O_4$–$xTiO_2$ ($x = 0.25$) ceramics (No. 4) reduces to −25.4 ppm/°C, which could result from the effect of $Zn_2Ti_3O_8$ phase in the system, as shown in Fig. 4(b). The $Q{\cdot}f$ value of No. 4 is twice more than that of No. 3 due to the higher bulk density of the former.

4. Conclusions

In the $(1-x)ZnAl_2O_4$–$xTiO_2$ system, LiCl and $ZnCl_2$ molten-salt process can prepare smaller and more homogenous grains than the solid-state reaction method, and can effectively lower its densification temperature. $Li_{2x}Zn_{(2-x)}Ti_3O_8$ (or $Zn_2Ti_3O_8$) low temperature phase exists easily in the calcined powder synthesized by molten-salt, and it reduces gradually until disappears with the increase of TiO_2 content or sintering temperature. In general, the ε_r value of the $(1-x)ZnAl_2O_4$–$xTiO_2$ ceramics synthesized by molten-salt process reduces slightly, and the density, $Q{\cdot}f$ and τ_f values deteriorate, however, they are closely related to the kind of molten-salt.

Acknowledgements

This work was supported by Program for New Century Excellent Talents in University (NCET-07-0329) and China Postdoctoral Science Foundation (CPSF-20080440925). The authors are grateful to the Analytical and Testing Center, Huazhong University of Science and Technology, for XRD and SEM analyses.

References

[1] M.-E. Song, J.-S. Kim, M.-R. Joung, S. Nahm, Y.-S. Kim, J.-H. Paik, B.-H. Choi, J. Am. Ceram. Soc. 91 (2008) 2747–2750.

[2] K.P. Surendran, M.T. Sebastian, M.V. Manjusha, J. Philip, J. Appl. Phys. 98 (2005) 044101.
[3] W. Lei, W.-Z. Lu, J.-H. Zhu, X.-H. Wang, Mater. Lett. 61 (2007) 4066–4069.
[4] W.-Z. Lu, W. Lei, J.-H. Zhu, F. Liang, Jpn. J. Appl. Phys. 46 (2007) L724–L726.
[5] W. Lei, W.-Z. Lu, J.-H. Zhu, X. Ye, Ceram. Int. 35 (2009) 277–280.
[6] X. Tian, L. Wan, K. Pan, C. Tian, H. Fu, K. Shi, J. Alloys Compd. 488 (2009) 320–324.
[7] Y. Wu, J. Du, K.L. Choy, L.L. Hench, J. Guo, Thin Solid Films 472 (2005) 150–156.
[8] Z. Li, S. Zhang, W.E. Lee, J. Eur. Ceram. Soc. 27 (2007) 3407–3412.
[9] B.W. Hakki, P.D. Coleman, IRE Trans. Microwave Theory Technol. 8 (1960) 402–410.
[10] W.L. Chen, Ph.D. Dissertation, Kunming University of Science and Technology, Kunming, China (2007).